Characteristics and Mechanisms of Pb(II) Sorption onto Fe-rich waste Water Treatment Residue (WTR): A potential sustainable Pb immobilisation technology for soils

Nina C. Finlay[1], Caroline L. Peacock[2], Karen A. Hudson-Edwards[3*], Karen L. Johnson[1]

[1] *Department of Engineering, Durham University, Durham DH1 3LE, UK.*

[2] *School of Earth and Environment, University of Leeds, Leeds LS2 9JT, UK.*

[3] *Environment & Sustainability Institute and Camborne School of Mines, University of Exeter, Penryn, Cornwall, TR10 9FE, UK.*

*Corresponding author: Karen A. Hudson-Edwards k.hudson-edwards@exeter.ac.uk

Keywords: Water treatment residue (WTR); lead; sorption; ferrihydrite; EXAFS.

Accepted version in: *Journal of Hazardous Materials*

Date of acceptance: 6 July 2020

ToC Art

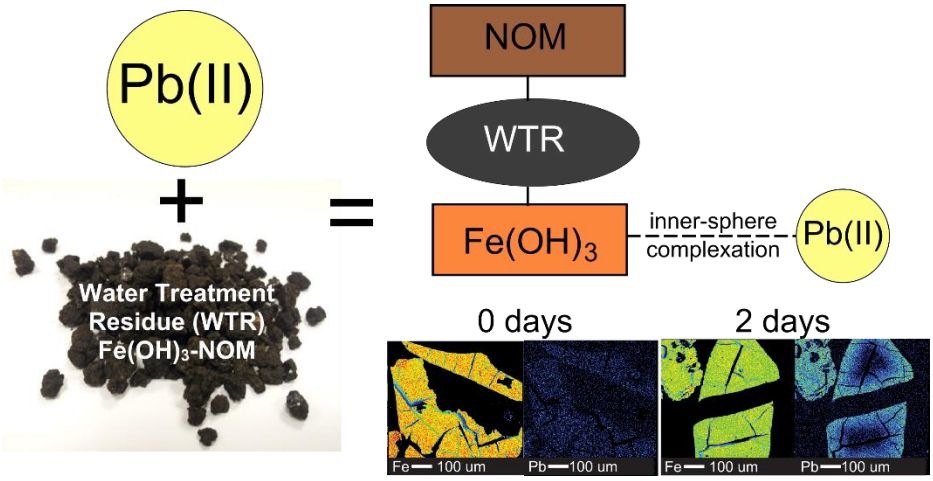

Abstract

Pb contamination of soils is a global problem. This paper discusses the ability of an Fe-rich waste, water treatment residual (WTR), to adsorb Pb(II). This was investigated using batch sorption experiments, X-ray diffraction, electron microprobe microanalysis, PHREEQC modelling and Extended X-ray Absorption Fine Structure (EXAFS) analysis. The WTR is composed of approximately 23 wt. % natural organic matter (NOM), 70 wt. % ferrihydrite and <10 wt. % silicate material. Pb(II) sorption to WTR was dependent on initial Pb(II) load, particle size, time and pH, but not on ionic strength. EXAFS analysis at the Pb L_{III}-edge confirmed that Pb(II) sorbed to WTR by co-existing bidentate edge-sharing and monodentate or corner-sharing complexes, with 2 O at ~2.31–2.34 Å, 1 Fe at ~3.32–3.34 Å, 2 Fe at ~3.97–3.99 Å and 1 Pb at ~3.82–3.85 Å. Linear combination showed that the Pb(II)-sorbed spectra were best fit with a ~0.9±0.1 and 0.1±0.1 contribution from Pb(II)-sorbed ferrihydrite and Pb(II)-sorbed humic acid end members, respectively. Overall, we show that Pb(II) sorbs via strong inner-sphere complexation of Pb(II) to the ferrihydrite component of the WTR, which itself is stable over a wide pH range. Therefore, we suggest that Fe-rich WTR wastes could be used as effective adsorbents in Pb(II)-contaminated soils to help ensure sustainable terrestrial ecosystems.

1. Introduction

Pb contamination in soils is a global problem. The UN has stated that healthy soils underpin all 17 Sustainable Development Goals (https://news.un.org/en/story/2018/08/1016902). This is specifically relevant to SDG12 (responsible production and consumption) and SDG15 (sustainable soils). Lead (Pb) is a well-known, non-biodegradable toxin for which there is no 'safe' level of exposure (Flora et al., 2012). Excessive intake of Pb can cause disorders of the central nervous, blood, digestive and renal systems (Kalia and Flora, 2005; Wani et al., 2015). Pb is a common contaminant in anthropogenically-impacted soils (Markus and McBratney, 2001; Carré et al., 2017 ; Shen et al., 2017). Many remediation schemes conducted to reduce this Pb-related risk to human health add ameliorants to soils to decrease Pb bioaccessibility and bioavailability (McCann et al., 2015). Examples of these include Mn oxide (McCann et al., 2015), fish bone phosphate (Freeman, 2012), clays (Wang et al., 2019), blast furnace slag (Wang et al., 2018a), Portland cement (Wang et al., 2018a, b), magnesium phosphate cement (Wang et al., 2018b), biochar (Mitzia et al., 2020), zero-valent iron (Mitzia et al., 2020) and water treatment residual (WTR) (Shen et al., 2019).These techniques have been shown to immobilise Pb very effectively, and most are low-cost and are widely available. WTR, however, is a waste product and so requires in many cases changes in legislation for its widespread use for Pb immobilisation. However, considering SDG12 (responsible use of resources), which covers reuse of waste materials, this could reduce treatment costs compared to the other techniques.

Water treatment residual (WTR) is a solid by-product generated by drinking-water treatment facilities worldwide and is commonly disposed of by landfill. It is a sludge-based waste which is produced during water purification as a consequence of the coagulation process. WTRs are known to contain high quantities of Fe or Al (oxyhydr)oxides and natural organic matter (NOM) (Castaldi et al., 2015). The capacity of Fe-rich WTR (Fe-WTR) as a sorbent of the oxyanion phosphate for potential control of nutrient-rich runoff and pollution prevention in downstream waters has been investigated (Makris et al., 2004a; Wang et al., 2013). Fe-WTR has also been found to have a high

capacity to immobilise metalloids such as As (Makris et al., 2009; Nagar et al., 2010), and metals including Cd, Cu, Pb and Zn (Chiang et al., 2012; Castaldi et al., 2015; Shen et al., 2019). Despite efforts to determine the mechanisms of uptake of Pb on Fe-WTR, no consensus has been made on these mechanisms, and on whether the Pb sorbs preferentially to the organic or inorganic components in this material (Castaldi et al., 2015; Shen et al., 2019). Such an understanding will help to assess WTR's sorbent capabilities for Pb, optimise adsorption pathways, design effective *in situ* stabilisation technologies and understand the long-term stability of the Pb-sorbed Fe-WTR. To address these issues, this study aimed to investigate the sorption behaviour, mechanisms and capacity of Fe-WTR for Pb. We present macroscopic and spectroscopic investigations in which batch sorption experiments were used to assess the Pb(II) sorption capacity and behaviour of WTR as a function of initial solution concentration, pH, ionic strength, contact time and particle size. We also compare the Pb sorption capacity and behaviour of WTR to that of its end member components ferrihydrite and humic acid, using X-ray absorption spectroscopy, in order to investigate the role of these in Pb(II) sorption. This study is essential to explore the potential of using WTR to immobilize Pb in terrestrial environments helping to improve terrestrial ecosystems (SDG15) whilst reusing a waste material (SDG12).

2. Materials and Methods

2.1. Materials

This study was carried out with water treatment works (WTR) residue, ferrihydrite (Fh) and natural organic matter (NOM). WTR was collected in 2011 from Broken Scar, a water treatment works facility managed by Northumbria Water Ltd in north-east England. Broken Scar WTW uses Fe-based anionic polyacrylamide with Na acrylic coagulants, and generates the largest quantity of WTR per annum in north-east England (3570 tonnes/yr dry solids in 2010-2011). Two-line ferrihydrite was used as the first of the model WTR end-members, and was synthesised following the method of Schwertmann and Cornell (2000) by the rapid hydrolysis of an Fe(III) salt solution. The

WTR and ferrihydrite were air-dried at 20 °C, ground using a mortar and pestle, sieved to < 63 μm and stored in the dark in clean screw-top polypropylene tubs.

Humic acid (HA) is often used to represent the hydrophobic fraction of NOM in laboratory experiments and it was considered appropriate for use as the second of the WTR end-member since it has been found that the hydrophobic, high molecular weight NOM fractions are more efficiently removed from raw water during coagulation treatment than the hydrophilic lower molecular weight fractions (Matilainen et al., 2010; Sharp et al., 2006). A small proportion of the carbon present in WTR originates from the organic polymer used in the flocculation process. At Broken Scar WTW, the polymer used was Flopam AN913 SEP (pers. comm, L. Dennis, NWL, 2011). In 2011, the average TOC concentration of the raw water feeding Broken Scar WTW was 10 mg/L (NWL data) and the average dose of Flopam polymer to raw water was set to not exceed 0.25 mg/L (pers. comm., SNF, 2012). Based on these figures, the amount of added carbon was calculated to be approximately 1 to 2% of the natural carbon. Therefore, HA (Sigma Aldrich, UK) was selected to represent the NOM fraction of WTR for subsequent Pb(II) sorption experiments. Humic acid (HA) was purchased from Sigma Aldrich, UK.

2.2. WTR, ferrihydrite and humic acid characterisation

The WTR was characterised for pH and EC (ISO 10390 method, 2005), C_{tot} and N_{tot} (COSTECH 4010 elemental combustion system), pseudo-total Fe and Pb concentrations (aqua regia digestion followed by ICP-MS and ICP-OES analysis), X-ray fluorescence (XRF; Spectro X--- Lab 2000), mineralogy (X-ray diffraction, XRD, Bruker AXS D8 Advance powder diffractometer using Cu-Kα radiation, 20 to 80 °2θ with a step size of 0.02 °2θ) and specific surface area (SSA; Micrometrics Tristar 3000 Gas Adsorption Analyser using BET method; Brunauer et al., 1938). A subsample of the WTR was air-dried at 20 °C, ground using a mortar and pestle, sieved to < 63 μm and stored in the dark in clean screw-top polypropylene tubs at room temperature prior to the batch Pb(II) sorption experiments.

Following preparation, the ferrihydrite precipitate was left to air dry before being ground to < 63 μm for sorption experiments. A subsample was freeze-dried and analysed by XRD and SSA using the methods described above. The HA was characterised using the SSA method described above.

2.2. Batch Pb(II) sorption experiments

Batch Pb(II) sorption experiments were carried out at room temperature (22±2 °C). Adsorption isotherm experiments designed to test the effect of initial Pb(II) loading were conducted at pH 5, with a 3 d contact time and a solid-solution ratio (SSR) of 10 g/L, using Pb(II) concentrations ranging from 10 to 300 mg/g (mg Pb(II)/g adsorbent) in 0.1 M $NaNO_3$. Experiments were also carried out at 0.01, 0.05, 0.1 and 0.5 M $NaNO_3$ to study the effect of ionic strength on Pb(II) sorption, using Pb(II) concentrations of 25 - 200 mg/g at pH 5, 3 d contact time and 10 g/L SSR. To measure the effect of contact time, experiments were run for 1 h, 2 h, 4 h, 8 h, 1 d, 2 d, 4 d, 7 d, 14 d and 21 d using Pb(II) concentrations of 25 - 200 mg/g in 0.1 M $NaNO_3$, at pH 5 and SSR of 10 g/L. The effect of pH was studied by conducting experiments at pH 3, 4, 5, 6 and 7 (to cover the sorption edge of Pb(II) on ferrihydrite; Bargar et al., 1997b; and the main pH range for most soils) using Pb(II) concentrations of 25 - 200 mg/g, 3 d contact time and SSR of 10 g/L. Suspensions of adsorbent in 0.1 M $NaNO_3$ were adjusted to the required pH prior to addition of Pb(II) stock solution and held at the set pH for the duration of the experiment with drop-wise additions of NaOH or HCl. Sieve-size fractions of <63 μm, 63-250 μm, 250-500 μm, 500 μm-1 mm and 1-2 mm were used to study the effect of particle size on Pb(II) sorption. Experiments were carried out at pH 5 in 0.1 M $NaNO_3$ and 3 d contact time and 10 g/L SSR using Pb(II) concentrations of 25 -200 mg/g. Pb(II) sorption experiments using Fh and HA were conducted at pH 5 using various Pb(II) concentrations in 0.1 M $NaNO_3$, 3 d contact time and SSR of 10 g/L.

Adsorption samples were prepared at 10 g/L solid:solution ratio (SSR) by adding the required volume of Pb(II) stock solution to 0.2 g adsorbent in 0.1 M $NaNO_3$. The pH was recorded

and adjusted to the required value by the drop-wise addition of 0.1 M NaOH or 0.1 M HCl whilst gently shaking the suspension. Suspensions were shaken at 150 rpm on a reciprocal shaker for the desired contact time, during which the pH was monitored and adjusted when necessary. The final pH was recorded before suspensions were centrifuged and filtered (0.45 μm cellulose acetate syringe filters) into 15 mL Corning polypropylene centrifuge tubes. Samples were acidified with concentrated HNO_3 and stored at 4 °C prior to analysis by atomic absorption spectroscopy (AAS). All experiments were performed in triplicate. Pb and Fe were analysed by AAS using a Varian SpectrAA 220FS instrument.

2.3. Electron microprobe microanalysis (EPMA)

Polished blocks of air-dried unreacted and Pb(II)-sorbed WTR samples were analysed by electron probe microanalysis (EPMA) and X-ray mapping using a Jeol 8100 Superprobe (WDS) with an Oxford Instrument Inca system (EDS). Energy spectral data were collected in the 0-20 eV range. Mapping of Fe, O and Pb was carried out using an accelerating voltage of 15 kV, current of 2.5 mA and beam diameter of 1 μm.

2.4. EXAFS analysis

Analysis of the Pb L_{III}-edge Extended X-ray Absorption Fine Structure (EXAFS) was carried out to investigate the speciation and bonding environment of the Pb(II) sorbed on the WTR, Fh and HA, on Station I20 at the Diamond Light Source Ltd, Didcot, UK. The samples used were those prepared at low loadings (10 mg Pb/g WTR, Fh or HA) and high loadings (200 mg Pb/g WTR, Fh or HA) at pH 5. To further investigate the influence of pH on sorption of Pb(II) on WTR, an additional sample at 10 mg Pb/g WTR at pH 4 was analysed.

XAS data were collected at the Pb L_{III}-edge (13.035 keV) for the Pb(II)-sorbed WTR, Fh and HA. Samples were presented to the X-ray beam as thick pastes approximately 1 mm thick, without dilution with boron nitride, were held in aluminium slides with predrilled sample slots, and

were sealed either side of the sample slots with Kapton tape. XAS data were collected from up to 36 scans in fluorescence mode using a Ge 9-element detector. A series of test scans were performed prior to data collection to confirm that there was no photo-redox or visible drying of the sample during data collection. Energy calibration was achieved by assigning the first inflection point the Au L_{III}-edge to 11.919 keV.

XAS data reduction was performed using ATHENA (Ravel and Newville, 2005) and the spectra were fit using DL_EXCURV (Tomic et al., 2005). The spectra were fit in k-space over 3 – 11 $Å^{-1}$, with no Fourier filtering during data analysis, and the fitting initially included full multiple scattering as coded in EXCURV98 (Binsted, 1998). Multiple scattering calculations require specification of the full three dimensional structure of the Pb coordination environment (i.e., atomic type and coordination of the surrounding atoms, and thus both Pb-atom bond lengths and bond angles). This was done using hypothetical model clusters with fixed atomic type and atomic coordination and with C1 symmetry, for various different possible Pb surface complexation coordination geometries (including mononuclear monodentate, mononuclear bidentate edge-sharing and mononuclear bidentate corner-sharing, where mononuclear refers to the number of Pb atoms in the surface complex). Comparison of the fits with and without multiple scattering showed that its inclusion offered no statistical improvement, and best fits are therefore presented without multiple scattering in a shell-by-shell approach.

The number of independent data points (N_{ind}) was determined using Stern's rule (Stern, 1993) as $2\Delta k\Delta R/\pi + 2$ (Booth and Hu, 2009) where Δk and ΔR are the range in k and R-space actually fitted; as such, $N_{ind} = 12$. The number of fitted parameters (N_{par}) was determined as the total number of parameters optimized during the various model refinements and was always less than N_{ind}. Typical errors associated with EXAFS modelling over the k-range used here are 15% and 25% for first and second shell coordination numbers, respectively, ±0.02 and 0.05 Å for first and second shell distances, respectively, and 15% and 25% for first and second shell Debye–Waller factors, re-

spectively (Binsted, 1998). The quality of the fits provided by the different model clusters was assessed using the EXAFS R-factor, with an absolute index of goodness of fit (used for comparing fit quality between clusters where N_{pars} was not equivalent) given by the reduced Chi^2 function (all as coded in EXCURV98; Binsted et al., 1996; Binsted, 1998).

Linear combination of the end-member first derivative spectra for Pb sorbed to ferrihydrite and humic acid was performed in ATHENA over -20 to 30 eV either side of the absorption edge, in order to provide an initial fit to the WTR spectra (using the 1 wt. % Pb sorbed end-members at pH 5 for WTR9_10 and WTR11_12, and the 20 wt. % Pb sorbed end-members at pH 5 for the WTR17_18). During the fitting, component sums were not constrained to equal one. The errors reported are those typically applied to 2-component mixtures during the linear combination of EXAFS data (at ± 10%; Kim et al., 2000).

3. Results

3.1. Characterisation of WTR, synthetic ferrihydrite and humic acid

XRD spectra for the WTR and synthetic ferrihydrite are shown in Figure 1. The scans yielded relatively poorly-resolved reflections with high backgrounds. Nevertheless, the two broad peaks at ~2.55 Å and 1.50 Å characteristic of 2-line ferrihydrite (Schwertmann and Cornell, 2000) were observed in both samples. The other peaks present in the WTR are attributed to quartz (3.34 and 1.82 Å) and goethite (4.19, 2.69, 2.46 and 1.72 Å). Based on an estimation of the C content of NOM as 58 wt. % (Rowell, 1994) and the approximate structural formula for ferrihydrite of $FeOOH_{0.4}.H_2O$, of which Fe constitutes 58 wt. % (Hiemstra and van Riemsdjik, 2009), it can be estimated that the WTR contains approximately 23 wt. % NOM and 70 wt. % ferrihydrite, with the rest (less than 10 wt. %) considered to be silicates from sand and clay inputs. The WTR contains 13.3 wt. % C_{tot}, 0.55 wt. % N_{tot}, 41.0 wt. % Fe, 88 mg/kg Pb (Table S1), and has a pH of 6.0 and EC of 307 µS/cm.

The specific surface area (SSA) of the WTR was measured to be 4.10 ± 0.09 m^2/g, similar to other reported values for ferrihydrite-NOM co-precipitates (e.g., Tampa, Florida WTR, 25 wt. % Fe, 14 wt. % C, SSA 3.9 m^2/g; Makris et al., 2004a). The SSA of the Fh was measured to be 280 ± 2.83 m^2/g, in agreement with previous research (200-350 m^2/g for synthetic 2-line ferrihydrite; Eggleton and Fitzpatrick, 1988; Schwertmann and Cornell, 2000). The SSA of the HA was measured as 0.97 ± 0.03 m^2/g, which is at the lower end of the range of values previous reported by Chiou et al. (1990; 0.61-18 m^2/g), but higher than that reported by Du et al. (2018; 0.2 m^2/g).

3.2. Batch Pb(II) sorption experiments

Figure 2a shows that the quantity of Pb(II) sorbed increased as the initial Pb(II) load increased from 10 to 300 mg Pb(II)/g < 63 µm diameter WTR at pH 5; however, the percentage Pb(II) sorbed decreased from 100% at 10 mg Pb(II)/g WTR to 45% at 300 mg Pb(II)/g WTR. Figure 2b demonstrates that the sorption of Pb(II) on WTR does not vary when the ionic strength is varied from 0.01 M to 0.5 M $NaNO_3$. Similar results were noted for Pb(II) sorption to ferrihydrite with a $NaNO_3$ electrolyte (Trivedi et al., 2003; Reich et al., 2010). Contact time has a significant effect on Pb(II) sorption on WTR with the effects being more pronounced with the higher initial Pb loading (e.g., 200 and 150 mg/kg Pb) experiments than with those with lower initial Pb loadings (Fig. 2c). Between 39% and 96% of the Pb(II) was sorbed within the first hour from systems loaded with between 25 and 200 mg Pb /g WTR (Fig. 2c). Thereafter the sorption of Pb(II) increased more slowly as contact time increased from 1 h to 21 days (Fig. 2c). Such biphasic kinetic behaviour for Pb(II) sorption has been reported for a range of sorbent materials including metal oxides (Strawn et al., 1998; Tiberg et al., 2013), organic matter (Strawn and Sparks, 2000) and other biosorbents (Gadd, 2009), and is attributed to instantaneous bulk diffusion and adsorption, followed by inner-sphere complexation (Grossl and Sparks, 1995; Hachiya et al., 1984). Particle size also had an effect on Pb(II) sorption, with sorption increasing as the WTR particle size increased from 1-2 mm to

< 63 µm. The effects were more pronounced at higher Pb(II) loadings up to 200 mg Pb(II)/g WTR (Fig. 2d).

Figure 3a demonstrates that Pb(II) sorption to WTR is pH dependent, and the effect of pH on sorption is more pronounced at higher Pb(II) loadings. The degree of sorption was lowest pH 3, approximately 60%, 50%, 30% and 24% of the 25, 50, 100 and 200 mg Pb(II)/g -loadings were sorbed, respectively, equating to 15, 24, 30 and 48 mg/g. Similar results were reported by Trivedi et al. (2003) and Gustafsson et al. (2011) for Pb(II) sorption on ferrihydrite. Pb(II) sorption increased to 100% between pH 5 and 6 for all Pb(II)-loaded systems and remained at 100% up to pH 8 (Fig. 3a). However, the actual quantity of Pb sorbed over the pH range was larger at the higher Pb loadings. Overall, the Pb sorption edges shifted to higher pH within increasing initial Pb load.

Less than 0.25% and <0.1% of the total Fe was released from the WTR at pH 3 and 4, respectively (Fig. 3a). By comparison, Pb(II)-ferrihydrite sorption experiments conducted by Gustafsson et al. (2011) showed more significant dissolution of Fe at low pH: up to 10% of the ferrihydrite dissolved at pH 3.0, and < 1% dissolved at pH 3.5.

Attempted fitting of sorption isotherm data for WTR, Fh and HA (Fig. 3a) to the equilibrium Langmuir (Langmuir, 1918) and Freundlich (Freundlich, 1906) isotherm models (Fig. 3b) gave a better fit for the Langmuir equation (R^2=0.994 compared to R^2=0.965). The Langmuir sorption capacity (q_{max}) was calculated to be 139 mg/g (0.68 mM/g), showing that WTR has a very high sorption capacity for Pb(II), similar to the Fe-WTR Pb(II) sorption capacity of 120 mg/g (0.579 mM/g) reported by Chiang et al. (2012). These results are similar to those of Kulczycki et al. (2005), who found that the Pb sorption capacity of *Bacillus subtilis*-Fh and E.-coli-Fh composites (103.5-141 mg/g) was much reduced in comparison to Fh (277 mg/g).

3.3. XRD and EMPA analysis

No Pb-bearing minerals were found by XRD analysis. The unreacted WTR is uniform and contains negligible Pb (Fig. 5a). Figures 5b and 5c show that < 2 mm WTR particles have sorbed

Pb(II) at 16 mg Pb(II)/ g and 100 mg Pb(II)/g loadings after 2 days, respectively, and that the concentration of Pb decreases towards the interior of the grains. By contrast, Pb(II) is dispersed throughout a < 63 μm Pb(II)-sorbed WTR particles that had undergone Pb(II) sorption at 200 mg Pb(II)/g loading for 3 d (Fig. 6a). Lead concentrations in this grain are fairly consistent across the grain at around 7-9 wt. % (average 8.5 wt. %), but are slightly higher towards the edges (Fig. 6a). After 21 d of Pb(II) sorption on a < 63 μm WTR particle at 200 mg/g Pb (II) loading, Pb is dispersed through the grain, but at higher concentrations (average 13.9 wt. %) than the 3 d experiment grain (Fig. 6b).

3.4. Geochemical modeling

The MINTEQv4 database in PHREEQC was used to predict the speciation of Pb in the experimental solutions (pH 5.5., 0.1 M $NaNO_3$, $aCO_2 = 10^{-3.5}$) used to generate the 10 mg Pb/g and 200 mg Pb/g samples. These calculations show that the experimental conditions are close to those thermodynamically predicted to favour precipitation of Pb hydroxide and Pb carbonate (Section S2). Specifically, in the 10 mg Pb/g and 200 mg Pb/g solutions $Pb(OH)_2$ is predicted to precipitate at pH 6.6 and 5.5, hydrocerrusite ($Pb_3(OH)_2(CO_3)_2$) (pH 5.1) at pH 6.5 and 5.1, and cerrusite ($PbCO_3$) is predicted to precipitate at pH 6.6 and 5.7, respectively (Section S2).

3.5. EXAFS analysis

The Fh_10mgPb/g_pH5 and Fh_200mgPb/g_pH5 spectra are visually very similar and reveal two distinct Pb sorption distances at ~ 3.3 Å and ~ 3.9 Å (Fig. 7). Given the similarity between these spectra, EXAFS indicates that the mechanism of Pb sorption to ferrihydrite at pH 5 appears to be independent of Pb loading. These spectra were best fit by shells representing 2 O at 2.31 – 2.33 Å, 1 Fe at 3.31 – 3.34 Å, 2 Fe at 3.93 – 3.95 Å and 1 Pb at 3.80 – 3.81 Å (Table 1). The O distance is in good agreement with other studies of Pb sorption on metal (hydr)oxides (Manceau et al., 1996; Bargar et al., 1997a, b; Bargar et al., 1998; Elzinga et al., 2001; Scheinost et al., 2001; Trivedi et al.,

2003; Du et al., 2018). The CN of 2 O for the first shell agrees with the findings of Tiberg et al. (2013) and Du et al. (2018), who studied the sorption of Pb(II) on ferrihydrite. The ~ 3.3 Å Pb-Fe distance is interpreted as a bidentate edge-sharing complex, where the literature to date shows that distances in the range ~ 2.9 – 3.5 Å arise from edge-sharing bidentate sorption of Pb ions to $Fe(OH)_6$ octahedra (e.g., Bargar et al., 1997b; Trivedi et al., 2003). The ~ 3.9 Å distance is interpreted as either a monodentate or corner-sharing complex (e.g., Bargar et al., 1997b). The coexistence of both the bidentate edge-sharing and monodentate or corner-sharing complexes in Pb-ferrihydrite sorption samples appears to be a function of pH, with Pb-ferrihydrite sorption samples prepared at pH < 5 showing evidence for the mixed sorption coordination environment (Trivedi et al., 2003) while Pb-iron (hydr)oxide sorption samples prepared at pH > 5 showing predominantly edge-sharing complexation (Bargar et al., 1997b; Trivedi et al., 2003). Inclusion of a shell consisting of 1 Pb at ~ 3.8 Å significantly improved the fits and we interpret this as Pb sorbed in Pb-Pb polynuclear complexes (Bargar et al., 1997a). The Pb distance is less likely to be due to the precipitation of a Pb crystalline or poorly crystalline phase (for example, $Pb(OH)_2$ (s)) because, despite the fact that the experimental conditions are close to those that are thermodynamically predicted to favour precipitation of Pb hydroxide and Pb carbonate (Table S2), the EXAFS spectra do not resemble those of any Pb(II) (hydr)oxide or carbonate precipitates present in the literature (e.g., Manceau et al., 1996; Bargar et al., 1997a).

Similar to the Pb-ferrihydrite spectra, the HA_10mgPb/g_pH5 and HA_200mgPb/g_pH5 spectra are visually very alike (Fig. 7), indicating that the mechanism of Pb sorption to humic acid at pH 5 appears to be independent of Pb loading. The EXAFS spectra are best fit by shells representing 2 O at ~ 2.31 – 2.33 Å and 2 C at 3.23 – 3.26 Å. The inclusion of the second shell of C atoms significantly improved the fit and is consistent with Pb complexed to HA via phenolic OH and possibly carboxylic COOH groups (Manceau et al., 1996; Du et al., 2018).

Visual comparison of the Pb-ferrihydrite, Pb-humic acid and Pb-WTR spectra indicates that the Pb-WTR spectra are visually most similar to the Pb-ferrihydrite spectra, and quite dissimilar to

the Pb-humic acid spectra (Fig. 7). Linear combination of the end-member spectra confirmed this visual comparison, and revealed that WTR_10mgPb/g_pH4.5, WTR_10mgPb/g_pH5 and WTR_200mgPb/g_pH5 were best fit with a ~ 0.9±0.1 and 0.1±0.1 contribution from the Pb-ferrihydrite and Pb-humic acid end-member spectra, respectively. Based on this result we fitted the Pb-WTR spectra adopting the same Pb coordination environment as fit for the Pb-ferrihydrite end-member sorption samples. The fits could not be improved by including a shell of C atoms, either instead of or in addition to the Pb-Fe and Pb-Pb shells. In summary we fitted 2 O at ~ 2.31 – 2.34 Å, 1 Fe at ~ 3.32 – 3.34 Å, 2 Fe at ~ 3.97 – 3.99 Å and 1 Pb at ~ 3.82 – 3.85 Å (Table 1).

4. Discussion

4.1. Controls on, and mechanisms of, Pb(II) uptake by, and incorporation in, WTR

Pb(II) sorption to WTR is dependent on initial Pb(II) load (Fig. 2a), particle size (Fig. 2b), time (Fig. 2c) and pH (Fig. 3a), but not ionic strength (Fig. 2b). The PHREEQC results suggest that Pb precipitation may be have been induced in the highest [Pb] sorption systems, but the Pb(II) solutions were added slowly and drop-wise to avoid introducing a shock load of Pb(II). Additionally, the isotherm (Fig. 4a) does not show characteristic precipitation features in that increasing Pb(II) concentrations did not result in a steep upturn in the graph which is the typical effect seen in a system controlled by precipitation (McBride, 1994). In addition, the Pb distance at ~ 3.8 Å for the WTR and Fh EXAFS fits (Fig. 7, Table 1) is not likely to be due to the precipitation of a Pb crystalline or poorly crystalline phase (for example, $Pb(OH)_2$ (s)) because, despite the fact that the experimental conditions are close to those that are thermodynamically predicted using PHREEQC to favour precipitation of Pb hydroxide and Pb carbonate (Section S2), the EXAFS spectra (Fig. 7) do not resemble those of any Pb(II) (hydr)oxide or carbonate precipitates present in the literature (Manceau et al., 1996; Bargar et al., 1997a). Therefore, the H-type isotherm (Fig. 4a), PHREEQC, XRD, EPMA (Fig. 5, 6) and EXAFS results (Fig. 7, Table 1) overall suggest that precipitation does

not play a major role in Pb(II) removal by WTR. Instead, our EXAFS fitting suggests that chemisorption of Pb(II) to surfaces of WTR components is the dominant mechanism for Pb(II) removal. This is supported by the good fit to the Langmuir equation (Fig. 4b), because the Langmuir isotherm models homogenous, monolayer adsorption, where each molecule has constant enthalpy and sorption activation energy and all sites possess equal affinity for the adsorbate (Foo and Hameed, 2010).

Our data also suggest that intraparticle diffusion may have controlled the second slow phase of sorption following the initial rapid Pb(II) uptake. For example, the uniformly Pb-distributed 21 d Pb(II)-sorbed < 63 μm WTR grain particle (Fig. 6b) may have resulted from diffusion of Pb from initial enrichment at the edges of the grain after 3 d (Fig. 6a). It is proposed that diffusion of Pb(II) ions into WTR may be hindered in places where pores are smaller or narrower and the pore connectivity is particularly constricted (cf., Makris et al., 2004b). This could result in a bottle-neck effect which reduces the rate of diffusion through such pores (Makris et al., 2004a). The rate of Pb(II) sorption would be expected to decline as the most accessible reactive sites are taken up and the remaining sorption sites become increasingly more difficult to reach, which is what is observed in this study (Fig. 5, 6). Furthermore, the initial Pb(II) loading affects the extent of diffusion, shown by the enrichment of Pb c. 50-80 μm into the 16 mg/g Pb(II)-loaded < 2 mm WTR grain (Fig. 5b) compared to the enrichment of Pb more than 100 μm into the 100 mg/g Pb(II)-loaded grain (Fig. 5c). These features suggesting that Pb diffuses further into the microporous WTR in the higher Pb(II)-loaded experiments in order to access available binding sites.

4.2. Controls on Pb(II) sorption by Fh and HA end-member WTR components

It was hypothesized that the Pb(II) sorption behavior of WTR would be intermediate to its end-member Fh and HA components, as proposed by other authors (Castaldi et al., 2015). HA has a lower pH_{pzc} (~2.5-3) than Fh (~7.5-8), suggesting that over the pH range of the experiments (3-7),

the net surface charge on HA would be more negative than the net surface charge on Fh. This suggests that HA would exhibit greater sorption capacity than Fh over the pH regime studied (cf., Moon and Peacock, 2011; Zhu et al., 2010). However, the sorption edge (Fig. 3b), isotherm (Fig. 4b) and EXAFS models (Fig. 7, Table 1) strongly suggest that Pb(II) sorption to WTR is dominated by inner-sphere complexation to the Fh end-member over the whole pH range of the experiments. The finding contrasts with the results of other studies which have found that metal sorption is influenced by both components in different parts of the pH regime; the presence of additional metal binding sites provided by the humic fraction, or new high affinity sites created when the humics sorb to the hydroxide surface (Moon and Peacock, 2013; Tipping et al., 1983; Zhu et al., 2010; Du et al., 2018). Our new finding has positive implications for the use of Fe-rich WTR in remediation schemes for stabilising metals such as Pb.

The fact that WTR has a lower sorption capacity than either of its end-members suggests that the reactivity of the NOM and the Fh has been reduced within the organo-mineral WTR composite. This may be due to intermixing of the Fh and NOM, which could protect both components from degradation and reduce their reactivity as a result of the binding and masking of surface sites. Additionally, the WTR may exhibit a more constrained, heavily cross-linked structure with a reduced pore network. Both of these effects would cause a reduction in Pb(II) sorption to WTR in comparison to its end-members. This is supported by work that has shown that NOM can mask Fh surfaces within organo-mineral composites (Franzblau, 2014; Kaiser and Guggenberger, 2000) therefore reducing the availability of Fh surface sites for metal sorption (Kulczycki et al., 2005; Small et al., 1999). The preferential binding of Pb(II) to the Fh component rather than the HA component may be a result of the HA not truly reflecting the NOM component of the WTR, or to strong binding between NOM and Fh surface functional groups that may result in a reduced number of available OM sites for sorption, altered surface charge on NOM which reduces its affinity for Pb(II) or a more constrained porous structure causing spatial inaccessibility between NOM and Pb(II).

The limited dissolution of Fe from the WTR during the Pb(II) sorption experiments suggests that the Fh is fairly stable within the WTR. This finding has positive implications for the use of WTR as an adsorbent in terrestrial environments, both because it is able to function as a Pb(II) sorbent across a wide range of pHs, and also that the WTR particles appear to remain stable over a wide pH range. Therefore, WTR waste may provide a cost-effective soil improvement technology for immobilising Pb in terrestrial environments helping to address both SDG 12 (responsible use of resources) and SDG15 (healthy soils in a sustainable terrestrial environment). In the UK, former Soil Guideline Values for Pb have been withdrawn as new scientific evidence on the toxicity of this element comes to light. However in the new more practical (but still strongly precautionary) guidance on when a Potentially Toxic Element like Pb presents a risk to site users, the lowest provisional Category for Screening Level (pC4SL; Defra, 2014) for Pb is 80 mg/kg (for allotment soils). Category 4 means that the land is not legally contaminated and the risk posed by the PTE of concern is low. The Pb content of the studied WTR (88 mg/kg) is marginally above this tightest pC4SL, and this may occasionally limit its appropriateness for remediation, particularly for soils where food will be produced. If soils contain considerably more Pb than this, the high sorption capability of the WTR could make the WTR a viable option especially in the case where all of the Pb would be immobilised.

5. Conclusions

In the present study Fe-rich WTR was explored as a potential in situ amendment for the remediation of Pb(II)-contaminated soils. Results demonstrated that the WTR is an effective Pb(II) sorbent, and that sorption was dependent on initial Pb(II) particle size, time and pH, but not on ionic strength. EXAFS modeling the Pb(II) mainly sorbed to the ferrihydrite component of WTR by forming co-existing bidentate edge-sharing and monodentate or corner-sharing complexes. Future work should focus on exploring the capacity for, and mechanisms of uptake of other potentially toxic metals in,

WTR, and on trialing WTR in contaminated field soils. This would help to address SDGs and to provide a sustainable application for WTR as an alternative to landfill disposal.

Author contributions

KLJ designed the research, NCF and KLJ conducted the batch experiments, KHE carried out the EPMA mapping and analysis, NCF, KHE and CLP conducted the EXAFS experiments, NCF and CLP analysed and modeled the EXAFS data and carried out the PHREEQC modeling, all authors wrote the manuscript.

Competing financial interests statement

The authors declare no competing financial interests.

Acknowledgements

We thank the three anonymous reviewers whose comments and suggestions improved the manuscript. We also thank Andy Beard (Birkbeck, University of London) and Frank Davies, Martin West, Amanda Hayton, Alison Clark, Kathryn Melvin, Neil Tunstall, Chris Longley, Steve Richardson, Kevin Longley, Helen Riggs and Leon Bowen (Durham) for technical assistance. We thank Roberto Boada Romero (Station Scientist, Diamond Light Source Ltd.) for support at Station I20. We thank Diamond Light Source for access to beamline I20 [STFC grant number SP4133] that contributed to the results presented here. The research was funded by EPSRC [grant numbers EP/E0441/17 and EP/1025782/1].

References

Bargar, J.R., Brown, G.E.Jr., Parks, G.A., 1997a. Surface complexation of Pb(II) at oxide-water interfaces: I. XAFS and bond-valence determination of mononuclear Pb(II) sorption products and surface functional groups on aluminum oxides. Geochim. Cosmochim. Acta 61, 2617-2637.

Bargar, J.R., Brown, G.E.Jr., Parks, G.A., 1997b. Surface complexation of Pb(II) at oxide-water interfaces: II. XAFS and bond-valence determination of mononuclear Pb(II) sorption products and surface functional groups on iron oxides. Geochim. Cosmochim. Acta 61, 2639-2652.

Bargar, J.R., Brown, G.E.Jr., Parks, G.A., 1998. Surface complexation of Pb(II) at oxide-water interfaces: III. XAFS and bond-valence determination of Pb(II) and Pb(II)-chloro adsorption complexes on goethite and alumina. Geochim. Cosmochim. Acta 62, 193-207.

Binsted, N., 1998. EXCURV98: The Manual. CLRC Daresbury Laboratory, Warrington, UK.

Binsted, N., Pack, M.J., Weller, M.T., Evans, J., 1996. Combined EXAFS and powder diffraction analysis. J. Am. Chem. Soc. 118, 10200–10210.

Booth, C.H., Hu, Y.-J., 2009. Confirmation of standard error analysis techniques applied to EXAFS using simulations. J. Phys.: Conf. Ser. 190, 1–6.

Brunauer, S., Emmett, P.H., Teller, E., 1938. Adsorption of gases in multimolecular layers. J. Am. Chem. Soc. 60, 309-319.

Carré F., Caudeville J., Bonnard R., Bert V., Boucard P., Ramel M., 2017. Soil contamination and human health: A major challenge for global soil security. In: Field D.J., Morgan C.L.S., McBratney A.B. (eds) Global Soil Security. Progress in Soil Science. Springer, Cham.

Castaldi, P., Silvetti, M., Garau, G., Demurtas, D., Deiana, S., 2015. Copper(II) and lead(II) removal from aqueous solution by water treatment residues. J. Hazard. Mater. 283, 140-147.

Chiang, Y.W., Ghyselbrecht, K., Santos, R.M., Martens, J.A., Swennen, R., Cappuyns, V., Meesschaert, B., 2012. Adsorption of multi-heavy metals onto water treatment residuals: Sorption capacities and applications. Chem. Eng. J. 2002, 405-415.

Chiou, C.T., Lee, J.F., Boyd, S.A., 1990. The surface area of soil organic matter. Environ. Sci. Technol. 24, 1164-1166.

Defra, 2014. Category 4 Screening Levels: The Project and the Facts. <https://www.southampton.gov.uk/policies/part%201%20-%20category%204%20screening%20levels%20-%202014%20sobra_sagta%20workshop%20presentation_tcm63-369734.pdf>

Du, H., Huang, Q., Lei, M., Tei, B., 2018. Sorption of Pb(II) by nanosized ferrihydrite organo-mineral composites formed by adsorption versus coprecipitation. ACS Earth Space Chem. 2, 556-564.

Eggleton, R.A., Fitzpatrick, R.W., 1988. New data and a revised structural model for ferrihydrite. Clays Clay Miner. 36, 111-124.

Elzinga, E.J., Peak. D., Sparks, D.L., 2001. Spectroscopic studies of Pb(II)-sulfate interactions at the goethite-water interface. Geochim. Cosmochim. Acta 65, 2219-2230.

Flora, G., Gupta, D., Tiwari, A., 2012. Toxicity of lead: A review with recent updates. Interdiscip. Toxicol. 5, 47-58.

Foo, K.Y., Hameed, B.H., 2010. Insights into the modeling of adsorption isotherm systems. Chem. Eng. J. 156, 2-10.

Franzblau, R.E., 2014. Metal ion adsorption onto bacteria-mineral composites. Unpublished M.Sc. thesis.

Freeman, K.S., 2012. Remediating soil lead with fish bones. Environ. Health Perspect. 120, a20-a21.

Freundlich, H., 1906. Over the adsorption in solution. J. Phys. Chem., 57, 1100-1107.

Gadd, G.M., 2009. Biosorption: critical review of scientific rationale, environmental importance and significance for pollution treatment. J. Chem. Technol. Biotechnol. 84, 13-28.

Grossl, P.R., Sparks, D.L., 1995. Evaluation of contaminant ion adsorption/desorption on goethite using pressure jump relaxation kinetics. Geoderma 67, 87-101.

Gustafsson, J.P., Tiberg, C., Edkymish, A., Kleja, D.B., 2011. Modelling lead(II) sorption to ferrihydrite and soil organic matter. Environ. Chem. 8, 485-492.

Hachiya, K., Sasaki, M., Ikeda, T., Mikami, N., Yasunaga, T., 1984. Static and kinetic studies of adsorption-desorption of metal ions on a. gamma-alumina surface. 2. Kinetic study by means of pressure-jump technique. J. Phys. Chem. 88, 27-31.

Hiemstra, T., Van Riemsdijk, W.H., 2009. A surface structural model for ferrihydrite I: Sites related to primary charge, molar mass, and mass density. Geochim. Cosmochim. Acta 73, 4423-4436.

Kalia, K., Flora, S.J., 2005. Strategies for safe and effective therapeutic measures for chronic arsenic and lead poisoning. J. Occup. Health 47, 1-21.

Kaiser, K., Guggenberger, G., 2000. The role of DOM sorption to mineral surfaces in the preservation of organic matter in soils. Org. Geochem. 31, 711-725.

Kim, W.B., Choi, S.H., Lee, J.S., 2000. Quantitative analysis of Ti-O-Si and Ti-O-Ti bonds in Ti-Si binary oxides by the linear combination of XANES. J. Phys. Chem. B 103, 8670-8678.

Kulczycki, E., Fowle, D., Fortin, D., Ferris, F., 2005. Sorption of cadmium and lead by bacteria-ferrihydrite composites. Geomicrobiol. J. 22, 299-310.

Langmuir, I., 1918. The adsorption of gases on plane surfaces of glass, mica and platinum. J. Am. Chem. Soc. 40, 1361-1403.

Manceau, A., Boisset, M.-C., Sarret, G., Hazemann, J.–L., Mench, M., Cambier, P., Prost, R., 1996. Direct determination of lead speciation in contaminated soils by EXAFS spectroscopy. Environ. Sci. Technol. 30, 1540-1552.

Makris, K.C., Harris, W.G., O'Connor, G.A., Obreza, T.A., 2004a. Phosphorus immobilization in micropores of drinking-water treatment residuals: Implications for long-term stability. Environ. Sci. Technol. 38, 6590-6596.

Makris, K.C., El-Shall, H., Harris, W.G., O'Connor, G.A., Obreza, T.A., 2004b. Intraparticle phosphorus diffusion in a drinking water treatment residual at room temperature. J. Colloid Interf. Sci. 277, 417-423.

Makris, K.C., Sarkar, D., Parsons, J.G., Datta, R., Gardea-Torresdey, J.L., 2009. X-ray absorption spectroscopy as a tool investigating arsenic (III) and arsenic (V) sorption by an aluminum-based drinking-water treatment residual. J. Hazard. Mat. 171, 980-986.

Markus, J., McBratney, A.B., 2001. A review of the contamination of soil with lead: II. Spatial distribution and risk assessment of soil lead. Environ. Int. 27, 399-411.

Matilainen, A., Vespäläinen, M., Sillanp, M., 2010. Natural organic matter removal by coagulation during drinking water treatment: A review. Adv. Colloid Interf. Sci. 159, 189-197.

McBride, M.B., 1994. Environmental Chemistry of Soils. Oxford University Press.

McCann, C.M., Gray, N.D., Tourney, J., Davenport, R.J., Wade, M., Finlay, N., Hudson-Edwards, K.A., Johnson, K.L., 2015. Remediation of a historically Pb contaminated soil using a model natural Mn oxide waste. Chemosphere 138, 211-217.

Mitzia, A., Vítková, M., Komáek, M., 2020. Assessment of biochar and/or nano zero-valent iron for the stablisation of Zn, Pb and Cd: A temporal study of solid phase geochemistry under changing soil conditions. Chemosphere 242, 125248.

Moon, E.M., Peacock, C.L., 2011. Adsorption of Cu (II) to *Bacillus subtilis*: a pH-dependent EX-AFS and thermodynamic modelling study. Geochim. Cosmochim. Acta 75, 6705-6719.

Moon, E.M., Peacock, C.L., 2013. Modelling Cu (II) adsorption to ferrihydrite and ferrihydrite-bacteria composites: Deviation from additive adsorption in the composite sorption system. Geochim. Cosmochim. Acta 104, 148-164.

Nagar, R., Sarkar, D., Makris, K.C., Datta, R., 2010. Effect of solution chemistry on arsenic sorption by Fe- and Al-based drinking-water treatment residuals. Chemosphere 78, 1028-1035.

Ravel, B., Newville, M., 2005. ATHENA, ARTEMIS, HEPHAESTUS: Data analysis for X-ray absorption spectroscopy using IFEFFIT. J. Synchrotron Radiat. 12, 537–541.

Reich, T.J., Das, S., Koretsky, C.M., Lund, T.J., Landry, C.J., 2010. Surface complexation modeling of Pb(II) adsorption on mixtures of hydrous ferric oxide, quartz and kaolinite. Chem. Geol. 275, 262-271.

Rowell, D.L., 1994. Soil Science: Methods and Applications. Longman Group Ltd, Longman Scientific & Technical.

Scheinost, A.C., Abend, S., Pandya, K.I., Sparks, D.L., 2001. Kinetic controls on Cu and Pb sorption by ferrihydrite. Environ. Sci. Technol. 35, 1090-1096.

Schwertmann, U. & Cornell, R.M., 2000. Iron Oxides in the Laboratory: Preparation and Characterisation, VCH Publishers.

Sharp, E.L., Parsons, S.A., Jefferson, B., 2006. Seasonal variations in natural organic matter and its impact on coagulation in water treatment Sci. Total Environ. 363, 183-194.

Shen, C., Zhao, Y., Li, W., Yang, Y., Liu, R., Morgen, D., 2019. Global profile of heavy metals and semimetals adsorption using drinking water treatment residual. Chem. Eng. J. 372, 1019-1027.

Shen, F., Liao, R., Ali, A., Mahar, A., Guo, D. Li, R., Sun, X., Awasthi, M.K., Wang, Q., Zhang, Z., 2017. Spatial distribution and risk assessment of heavy metals in soil near a Pb/Zn smelter in Feng County, China. Ecotoxicol. Environ. Safety 139, 254-262.

Small, T.D., Warren, L.A., Roden, E.E., Ferris, F.G., 1999. Sorption of strontium by bacteria, Fe (III) oxide, and bacteria-Fe (III) oxide composites. Environ. Sci. Technol. 33, 4465-4470.

Stern, E.A., 1993. Number of relevant independent points in X-ray absorption fine-structure spectra. Phys. Rev. B 48, 9825–9827.

Strawn, D.G., Sparks, D.L., 2000. Effects of soil organic matter on the kinetics and mechanisms of Pb (II) sorption and desorption in soil. Soil Sci. Soc. Am. J. 64, 144-156.

Strawn, D.G., Scheidegger, A.M., Sparks, D.L., 1998. Kinetics and mechanisms of Pb(II) sorption and desorption at the aluminium oxide-water interface. Environ. Sci. Technol. 32, 2596-2601.

Tiberg, C., Sjöstedt, C., Persson, I., Gustafsson, J.P., 2013. Phosphate effects on copper(II) and lead(II) sorption to ferrihydrite. Geochim. Cosmochim. Acta 120, 140-157

Tipping, E., Griffith, J., Hilton, J., 1983. The effect of adsorbed humic substances on the uptake of copper (II) by goethite. Croatica Chemica Acta, 56, 613-621.

Tomic, S., Searle, B. G., Wander, A., Harrison, N.M., Dent, A.J., Mosselmans, J.W.F., Ingelsfield, J.E., 2005. New Tools for the Analysis of EXAFS: The DL_EXCURV Package. CCLRC Technical Report DLTR-2005-001, Daresbury, UK.

Trivedi, P., Dyer, J.A., Sparks, D.L., 2003. Lead sorption onto ferrihydrite. 1. A macroscopic and spectroscopic assessment. Environ. Sci. Technol. 37, 908-914.

Wang, C., Bai L., Pei Y., 2013. Assessing the stability of phosphorus in lake sediments amended with water treatment residuals. J. Environ. Manage. 122, 31-36.

Wang, L., Cho, D.-W., Tsang, D.C.W., Cao, X., Hou, D., Shen, Z., Alessi, D.S., Ok, Y.S., Poon, C.S., 2019. Green remediation of As and Pb contaminated soil using cement-free clay-based stabilization/solidification. Environ. Int. 126, 336-345.

Wang, L., Yu, K., Li, J.-S., Tsang, D.C.W., Poon, C.S., Yoo, J.-C., Baek, K., Ding, S., Hou, D., Dai, J.-G., 2018a. Low-carbon and low-alkalinity stabilization/solidification of high-Pb contaminated soil. Chem. Eng. J. 351, 418-427.

Wang, Y.-S., Dai, J.-G., Wang, L., Tsang, D.C.W., Poon, C.S., 2018b. Influence of lead on stabilization/solidification by ordinary Portland cement and magnesium phosphate cement. Chemosphere 190, 90-96.

Wani, A.L., Ara, A., Usmani, J.A., 2015. Lead toxicity: A review. Interdiscip. Toxicol. 8, 55-64.

Zhu, J., Pigna, M., Cozzolino, V., Caporale, A.G., Violante, A., 2010. Competitive sorption of copper(II), chromium(III) and lead(II) on ferrihydrite and two organomineral complexes. Geoderma 159, 409-416.

TABLES

Table 1. EXAFS fits for Pb(II) sorbed to ferrihydrite (Fh), humic acid (HA) and WTR.

Sample	N_O R (Å) $2\sigma^2$ (Å)	N_{Fe} R (Å) $2\sigma^2$ (Å)	N_{Fe} R (Å) $2\sigma^2$ (Å)	N_{Pb} R (Å) $2\sigma^2$ (Å)	N_C R (Å) $2\sigma^2$ (Å)	EF	R-factor (%)	Reduced χ^2
Fh_10mgPb/g_pH5	2.0 2.33 0.022	1.0 3.31 0.028	2.0 3.95 0.035	1.0 3.81 0.017	-	10.8	28.6	21.0
Fh_200mgPb/g_pH5	2.0 2.31 0.025	1.0 3.34 0.032	2.0 3.93 0.037	1.0 3.80 0.022	-	9.2	26.1	18.1
HA_10mgPb/g_pH5	2.0 2.36 0.021	-	-	-	2.0 3.26 0.027	9.8	32.5	11.4
HA_200mgPb/g_pH5	2.0 2.35 0.031	-	-	-	2.0 3.23 0.037	11.2	26.4	13.8
WTR_10mgPb/g_pH4.5	2.0 2.34 0.025	1.0 3.34 0.039	2.0 3.99 0.040	1.0 3.85 0.018	-	10.4	34.4	26.0
WTR_10mgPb/g_pH5	2.0 2.33 0.026	1.0 3.32 0.036	2.0 3.97 0.035	1.0 3.84 0.013	-	10.5	33.1	25.9
WTR_200mgPb/g_pH5	2.0 2.31 0.028	1.0 3.33 0.038	2.0 3.97 0.037	1.0 3.82 0.025	-	9.9	28.8	21.7

N = number of atoms in coordination shell; R = Pb-atom bond distance; σ^2 = Debye-Waller factor; EF = Fermi energy; R-factor = EXAFS goodness of fit; Reduced χ^2 = EXAFS absolute goodness of fit.

FIGURES

Figure 1. XRD spectra for WTR and synthetic ferrihydrite. Major d-spacings are indicated for ferrihydrite (Fh), quartz (Qtz) and goethite (Goe).

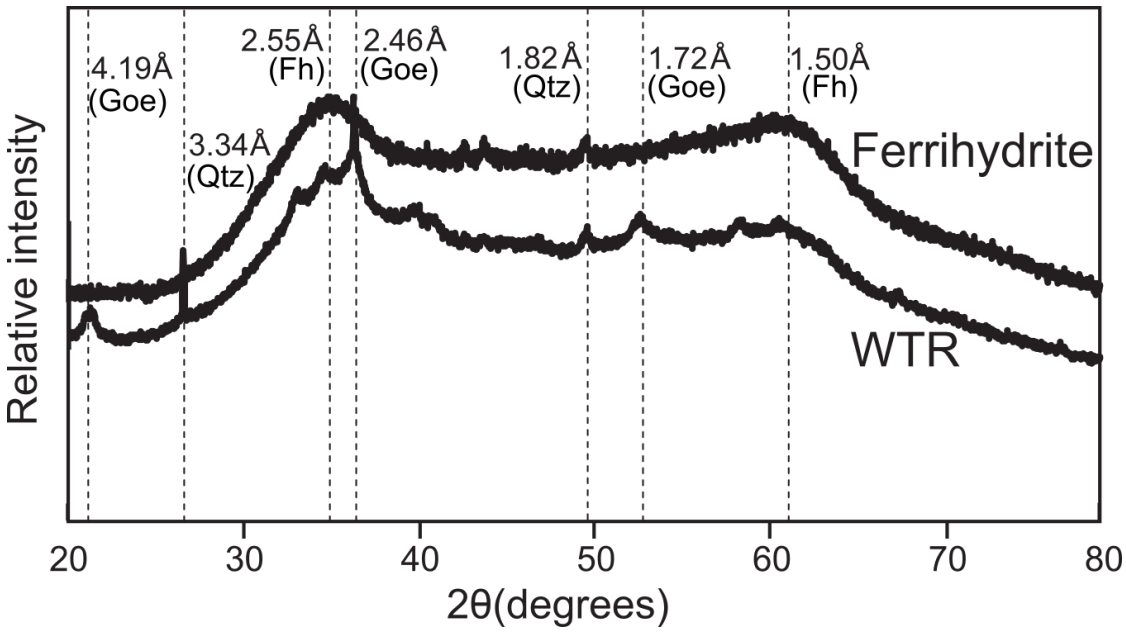

Figure 2. Effects of initial Pb load, ionic strength, contact time and particle size on Pb(II) sorption to WTR. (a) Effect of initial Pb load (mg Pb/g). pH = 5, I = 0.1 M $NaNO_3$, contact time 3 d, m/V = 10 g/L, T = 22 ± 2ºC, < 63 µm diameter WTR grains; (b) Effect of ionic strength. Pb load 25-200 mg Pb(II)/g,, pH = 5, I = 0.1 M $NaNO_3$, contact time 3 d, m/V = 10 g/L, T = 22 ± 2ºC, < 63 µm diameter WTR grains; (c) Effect of contact time. Pb load 25-200 mg Pb(II)/g,, pH = 5, I = 0.1 M $NaNO_3$, contact time 3 d, m/V = 10 g/L, T = 22 ± 2ºC, < 63 µm diameter WTR grains; (d) Effect of particle size. Pb load 25-200 mg Pb(II)/g, pH = 5, I = 0.1 M $NaNO_3$, contact time 3 d, m/V = 10 g/L, T = 22 ± 2ºC.

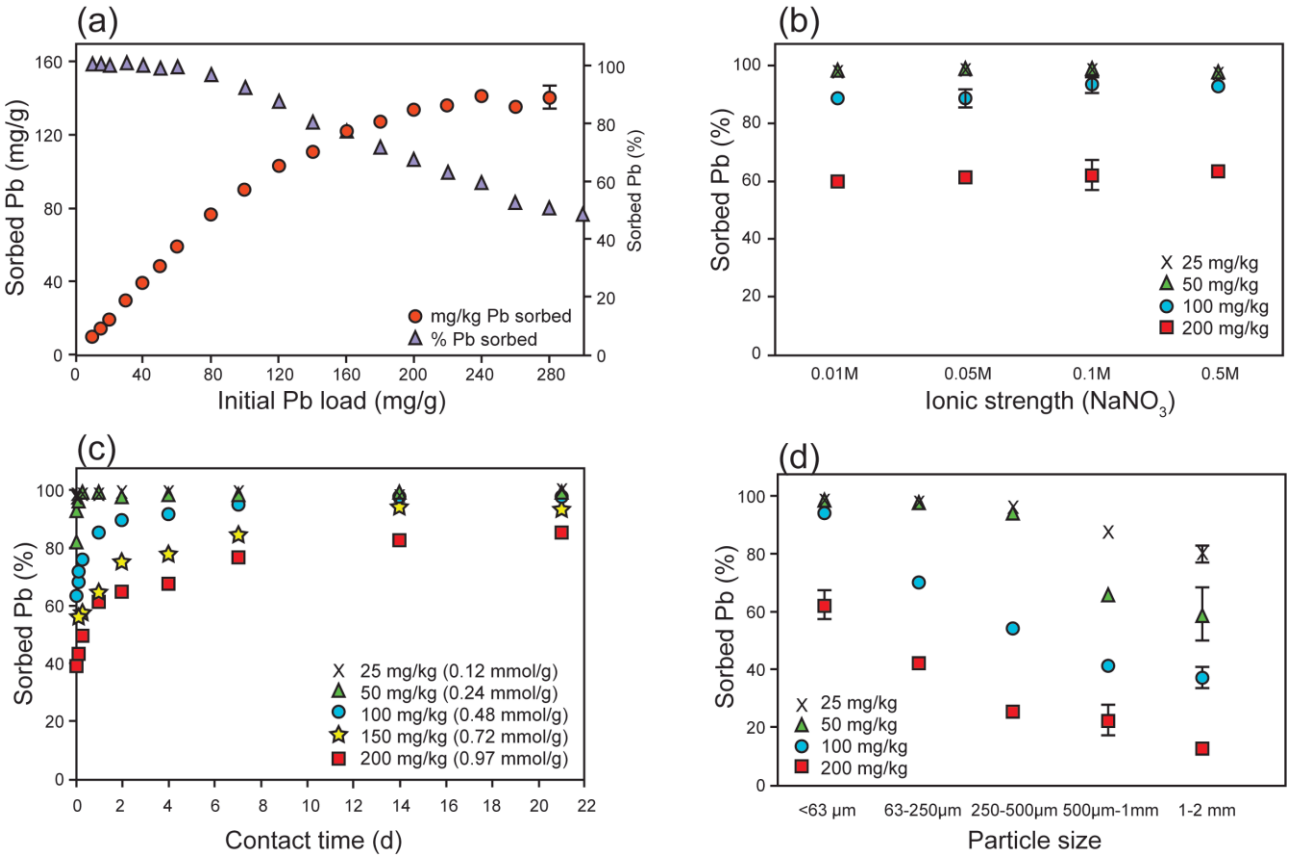

Figure 3. Effect of pH on Pb sorption to (a) WTR and (b) WTR, ferrihydrite (Fh) and humic acid (HA).

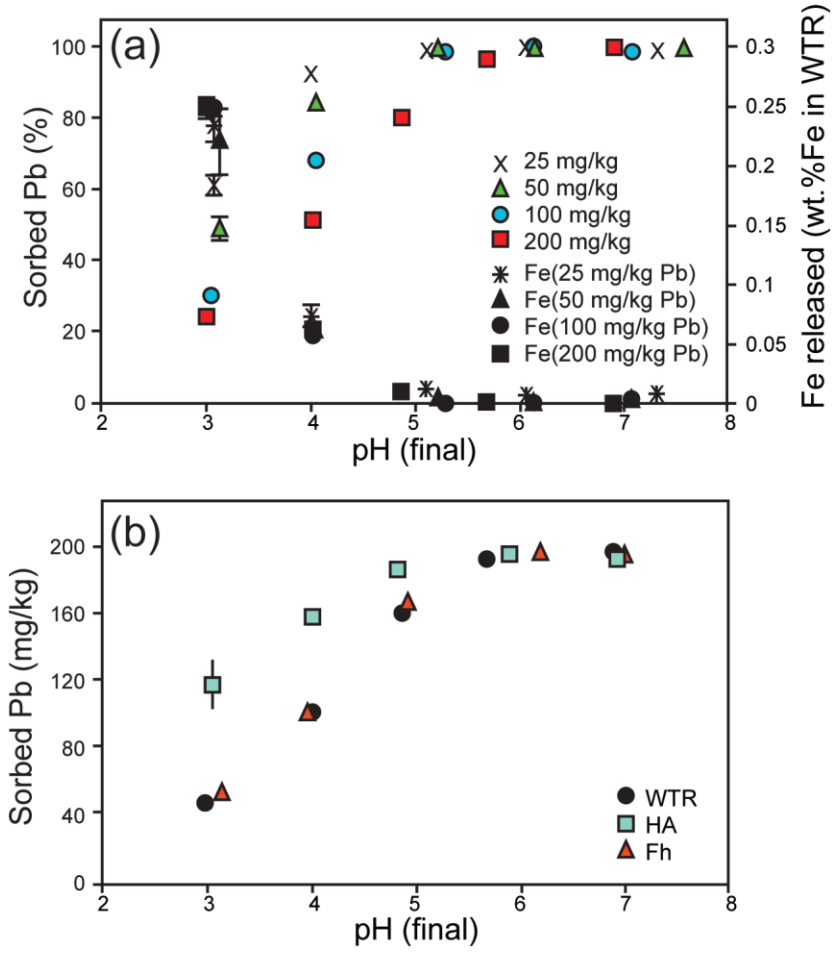

Figure 4. Adsorption of Pb(II) to WTR, HA and Fh. (a) adsorption isotherms; (b) Langmuir fits.

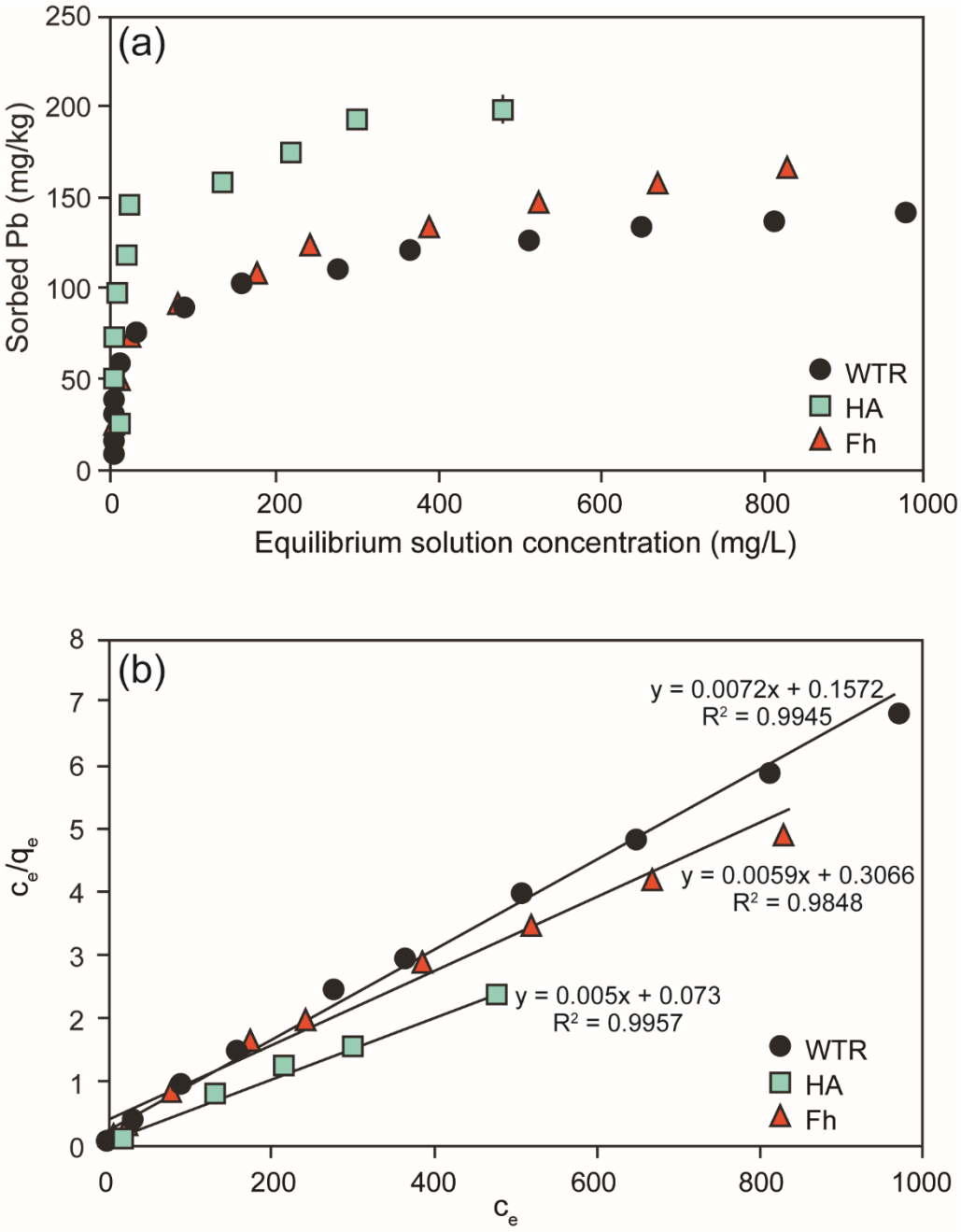

Figure 5. X-ray electron microprobe (EPMA) maps of (a) untreated < 2 mm diameter WTR grains, and Pb-sorbed < 2 mm diameter WTR grains at loadings of (b) 16 mg/g Pb and (c) 100 mg/g Pb, reacted for 2 days. CP: backscatter image, O: oxygen, Fe: iron, Pb: lead.

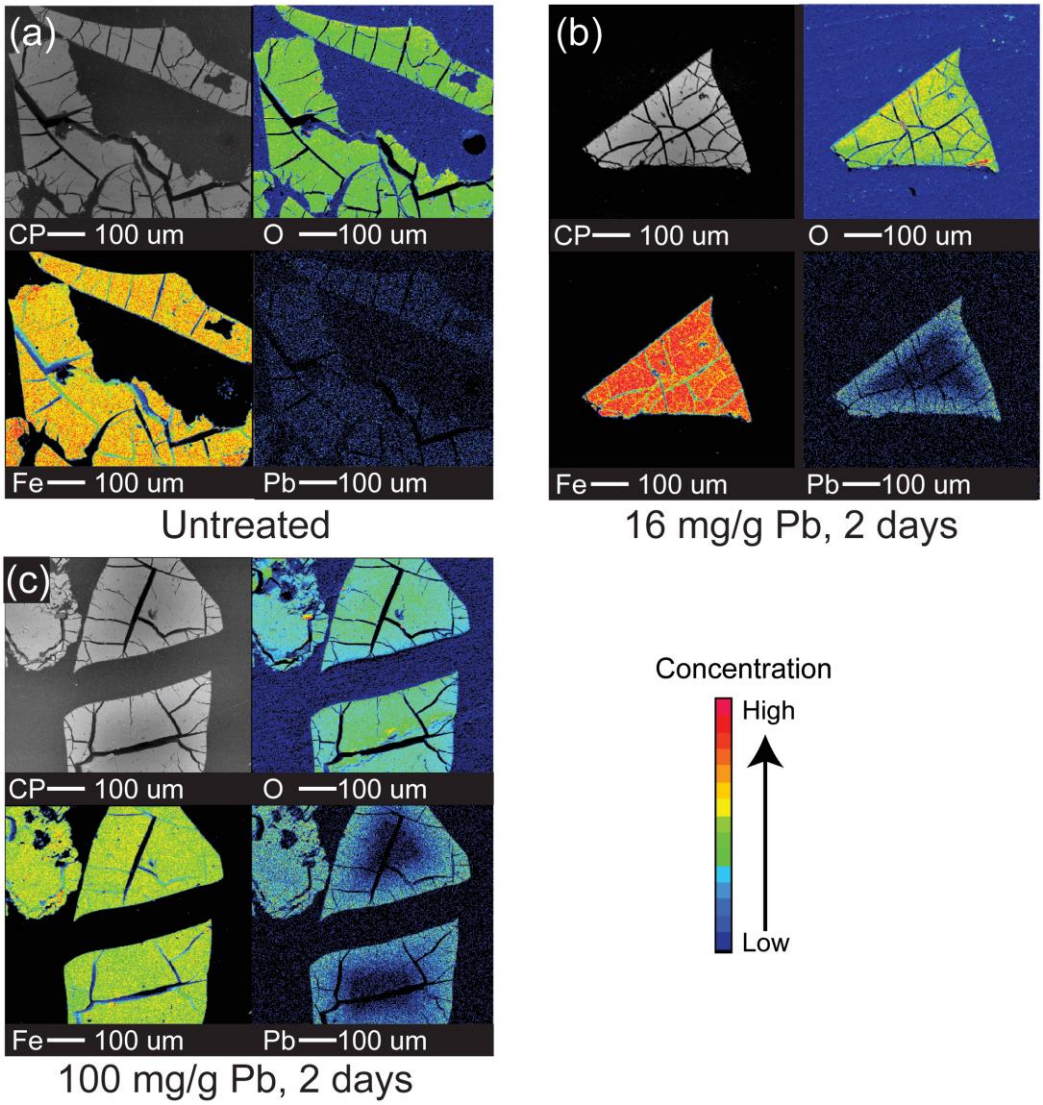

Figure 6. X-ray electron microprobe (EPMA) maps of Pb-sorbed < 63 µm diameter grains at 200 mg/g loadings. Red lines show location of microprobe line analyses across grains; the corresponding plots of wt. % Fe and wt. % Pb for these are shown below the maps. (a) Experiments reacted for 3 days; (b) experiments reacted for 21 days. CP: backscatter image, O: oxygen, Fe: iron, Pb: lead.

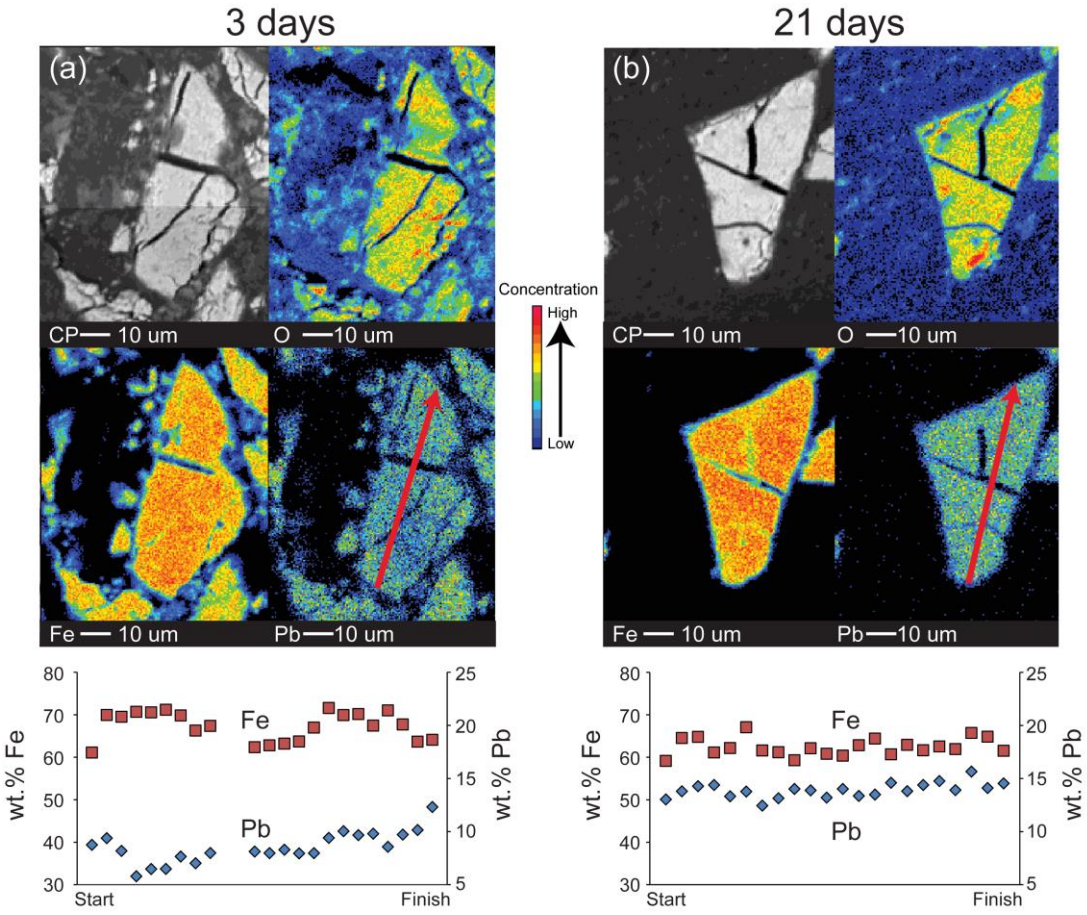

Figure 7. Lead L_{III}-edge EXAFS spectra for Pb(II) adsorbed on WTR, ferrihydrite (Fh) and humic acid (HA). (A) $k^3\chi$ (k) functions; (B) corresponding RSFs (uncorrected phase shift). The experimental data (solid line) are fitted (dashed line) using the parameters described in the text.

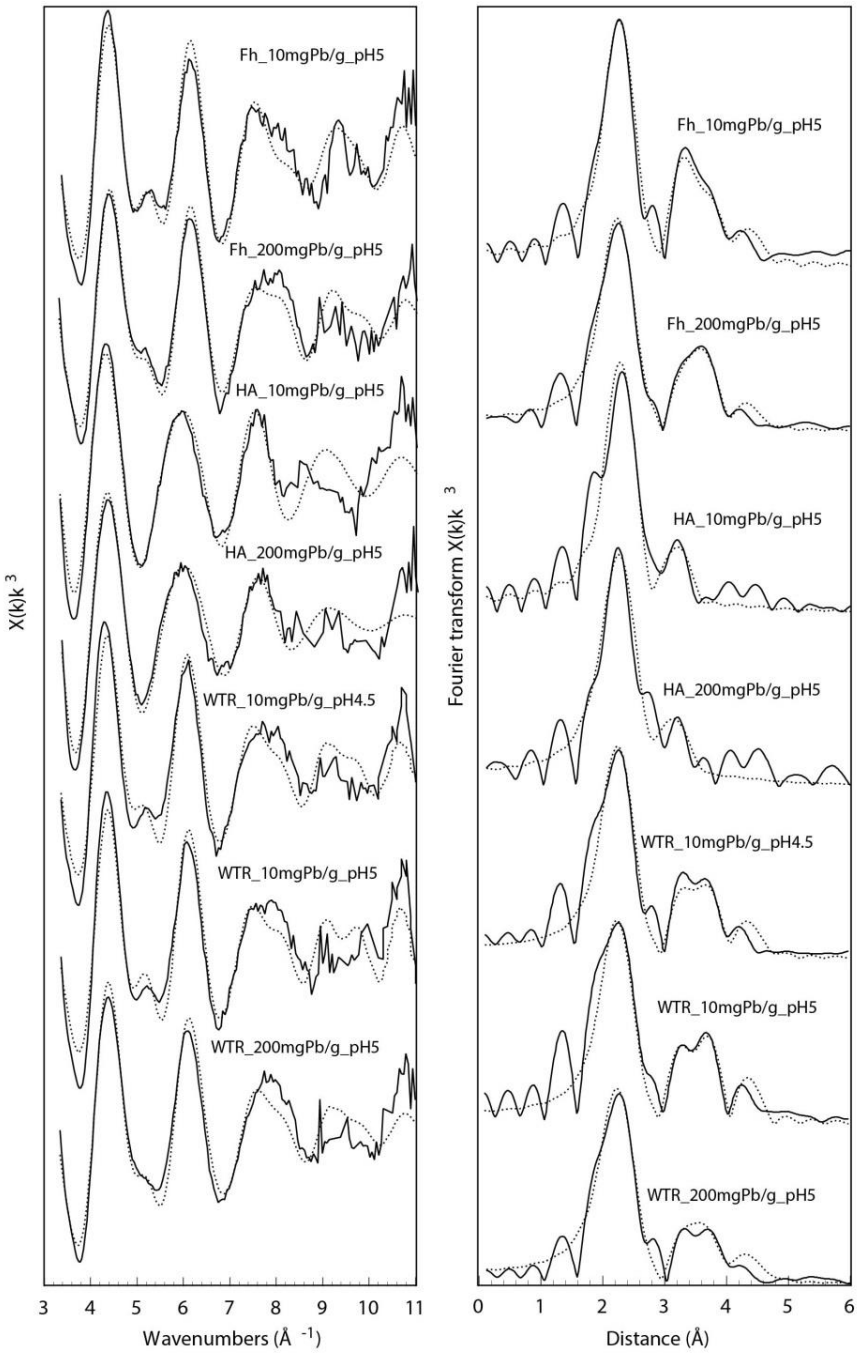

Characteristics and Mechanisms of Pb(II) Sorption onto Fe-rich waste Water Treatment Residue (WTR):

A potential sustainable Pb immobilisation technology for soils

SUPPLEMENTARY INFORMATION

Nina C. Finlay[1], Caroline L. Peacock[2], Karen A. Hudson-Edwards[3*], Karen L. Johnson[1]

[1] *Department of Engineering, Durham University, Durham DH1 3LE, UK.*

[2] *School of Earth and Environment, University of Leeds, Leeds LS2 9JT, UK.*

[3] *Environment & Sustainability Institute and Camborne School of Mines, University of Exeter, Penryn, Cornwall, TR10 9FE, UK.*

*Corresponding author: Karen A. Hudson-Edwards k.hudson-edwards@exeter.ac.uk

Keywords: Water treatment residue (WTR); lead; sorption; ferrihydrite; EXAFS.

Accepted version in: *Journal of Hazardous Materials*

Date of acceptance: 6 July 2020

Section S1. Geochemical characteristics of WTR.

Table S1. Geochemical characteristics of WTR.

Analyte	Analytical Method	Unit	WTR
C	Combustion	wt. %	13
N	Combustion	wt. %	0.55
Al	XRF	wt. %	0.3
Fe	Aqua regia + ICP-OES	wt. %	41
Si	Aqua regia digestion + ICP-MS	wt. %	0.8
Ca	XRF	wt. %	0.9
Mn	XRF	mg/kg	990
K	XRF	mg/kg	310
Mg	XRF	mg/kg	270
P	XRF	mg/kg	510
As	XRF	mg/kg	5.8
Pb	XRF	mg/kg	88
Zn	XRF	mg/kg	210

Section S2. PHREEQC Modelling

Pb solid	**Equation for precipitate formation**	**Log k**
Massicot	$Pb^{2+} + H_2O = PbO + 2H^+$	-12.894
Litharge	$Pb^{2+} + H_2O = PbO + 2H^+$	-12.694
$PbO:0.33H_2O$	Pb^{2+} + 1.33H2O = $PbO:0.33H_2O + 2H^+$	-12.98
$Pb(OH)_2$	$Pb^{2+} + 2H_2O = Pb(OH)_2 + 2H^+$	-8.15
$Pb_2O(OH)_2$	$2Pb^{2+} + 3H_2O = Pb_2O(OH)_2 + 4H^+$	-26.188
Cerrusite	$Pb^{2+} + CO_3^{2-} = PbCO_3$	13.13
Pb_2OCO_3	$2Pb^{2+} + H_2O + CO_3^{2+} = Pb_2OCO_3 + 2H^+$	0.5578
$Pb_3O_2CO_3$	$3Pb^{2+} + CO_3^{2+} +2H_2O = Pb_3O_2CO_3 + 4H^+$	-11.02
Hydrocerrusite	$3Pb^{2+} + 2H_2O + 2CO_3^{2+} = Pb_3(OH)_2(CO_3)_2 + 2H^+$	18.7705
$Pb_{10}(OH)_6O(CO_3)_6$	$10Pb^{2+} + 6CO_3^{2+} + 7H_2O = Pb_{10}(OH)_6OCO_{36} + 8H^+$	8.76

<u>PHREEQC Outputs</u>

--- --- --- --- --- --- --- --- --- --- --- --- --- --- --- --- --- ---

Reading data base.

--- --- --- --- --- --- --- --- --- --- --- --- --- --- --- --- --- ---

SOLUTION_MASTER_SPECIES
SOLUTION_SPECIES
SOLUTION_SPECIES
PHASES
PHASES
SURFACE_MASTER_SPECIES
SURFACE_SPECIES
END

--- ---

Reading input data for simulation 1.

--- ---

TITLE Speciating Pb in 0.1M NaNO3 in atm.
SOLUTION_SPECIES
Pb+2 + H2O = PbOH+ + H+

log_k --- 7.597

Pb+2 + 2H2O = Pb(OH)2 + 2H+
log_k --- 17.094
Pb+2 + 3H2O = Pb(OH)3--- + 3H+
log_k --- 28.091
2Pb+2 + H2O = Pb2OH+3 + H+
log_k --- 6.397
3Pb+2 + 4H2O = Pb3(OH)4+2 + 4H+
log_k --- 23.888
Pb+2 + 4H2O = Pb(OH)4--- 2 + 4H+
log_k --- 39.699
4Pb+2 + 4H2O = Pb4(OH)4+4 + 4H+
log_k --- 19.988
Pb+2 + NO3--- = PbNO3+
log_k 1.17
Pb+2 + 2NO3--- = Pb(NO3)2
log_k 1.4
Pb+2 + 2CO3--- 2 = Pb(CO3)2--- 2
log_k 9.938
Pb+2 + CO3--- 2 = PbCO3
log_k 6.478
Pb+2 + CO3--- 2 + H+ = PbHCO3+
200
log_k 13.2
PHASES
Pb(OH)2(s)
Pb(OH)2 + 2H+ = Pb+2 + 2H2O
log_k 8.15
Fix_pH
H+ = H+
log_k 0
SOLUTION 1 A: Speciation in pure water
pH 7
units mol/kgw
Pb 4.826e--- 05
END
--- --- --- --- ---
TITLE
--- --- --- --- ---
Speciating Pb in 0.1M NaNO3 in atm.
--- ---
--- --- --- --- ---
Beginning of initial solution calculations.
--- ---
--- --- --- --- ---
Initial solution 1. A: Speciation in pure water
--- --- --- --- --- --- --- Solution composition--- --- --- --- --- --
Elements Molality Moles

Pb 4.826e--- 05 4.826e--- 05

--- --- --- --- --- --- --- Description of solution--- --- --- --- --- --

pH = 7.000
pe = 4.000
Activity of water = 1.000

Ionic strength = 8.233e--- 05

Mass of water (kg) = 1.000e+00

Total alkalinity (eq/kg) = 9.561e--- 06

Total carbon (mol/kg) = 0.000e+00
Total CO2 (mol/kg) = 0.000e+00
Temperature (deg C) = 25.000

Electrical balance (eq) = 8.696e--- 05

Percent error, 100*(Cat--- |An|)/(Cat+|An|) = 99.77

Iterations = 4
Total H = 1.110137e+02
Total O = 5.550684e+01

- --- --- --- --- --- --- Distribution of species--- --- --- --- ---

Log Log Log
Species Molality Activity Molality Activity Gamma

OH--- 1.018e--- 07 1.007e--- 07 --- 6.992 --- 6.997 --- 0.005

H+ 1.011e--- 07 1.000e--- 07 --- 6.995 --- 7.000 --- 0.005

H2O 5.551e+01 1.000e+00 1.744 --- 0.000 0.000

H(0) 1.416e--- 25

H2 7.079e--- 26 7.079e--- 26 --- 25.150 --- 25.150 0.000
201
O(0) 0.000e+00

O2 0.000e+00 0.000e+00 --- 41.995 --- 41.995 0.000

Pb 4.826e--- 05

Pb+2 3.872e--- 05 3.713e--- 05 --- 4.412 --- 4.430 --- 0.018

PbOH+ 9.490e--- 06 9.391e--- 06 --- 5.023 --- 5.027 --- 0.005

Pb(OH)2 2.990e--- 08 2.990e--- 08 --- 7.524 --- 7.524 0.000

Pb2OH+3 6.075e--- 09 5.526e--- 09 --- 8.216 --- 8.258 --- 0.041

Pb3(OH)4+2 6.909e--- 10 6.625e--- 10 --- 9.161 --- 9.179 --- 0.018

Pb4(OH)4+4 2.312e--- 10 1.954e--- 10 --- 9.636 --- 9.709 --- 0.073

Pb(OH)3--- 3.043e--- 12 3.011e--- 12 --- 11.517 --- 11.521 --- 0.005

Pb(OH)4--- 2 7.744e--- 17 7.425e--- 17 --- 16.111 --- 16.129 --- 0.018

- --- --- --- --- --- --- --- --- --- Saturation indices--- --- --- --- ---

Phase SI log IAP log KT

Fix_pH --- 7.00 --- 7.00 0.00 H+

Litharge --- 3.12 9.57 12.69 PbO

Massicot --- 3.32 9.57 12.89 PbO

Minium --- 22.81 50.71 73.52 Pb3O4

O2(g) --- 39.09 44.00 83.09 O2

Pb(OH)2 1.42 9.57 8.15 Pb(OH)2
Pb(OH)2(s) 1.42 9.57 8.15 Pb(OH)2

Pb2O(OH)2 --- 7.05 19.14 26.19 Pb2O(OH)2

Pb2O3 --- 19.90 41.14 61.04 Pb2O3

Pbmetal --- 16.68 --- 12.43 4.25 Pb

PbO:0.3H2O --- 3.41 9.57 12.98 PbO:0.33H2O

Plattnerite --- 18.03 31.57 49.60 PbO2

--- --- --- --- --- --- --- --- --- --- --- --- --- --- --- --- ---

End of simulation.

--- --- --- --- --- --- --- --- --- --- --- --- --- --- --- --- ---

--- ---

Reading input data for simulation 2.

--- ---

SOLUTION 2 B: Speciation in NaNO3 solution
pH 7
units mol/kgw

Pb 4.826e--- 05

Na 0.1
N(5) 0.1 charge
END

PHREEQC OUTPUT SUMMARY

Massicot does not form between pH 1 and 10 // pH 9.1
Litharge does not form between pH 1 and 10 // pH 8.9
$PbO:0.33H_2O$ does not form between pH 1 and 10 // pH 9.2
$Pb(OH)_2$ pH 6.6 // 5.5
$Pb_2O(OH)_2$ does not form between pH 1 and 10 // pH 9.4
Cerrusite pH 6.6 // 5.7
Pb_2OCO_3 pH 8.4 // 6.7
$Pb_3O_2CO_3$ pH 8.5 // 7.0
Hydrocerrusite pH 6.5 // 5.1
$Pb_{10}(OH)_6O(CO_3)_6$ does not form between pH 1 and 10 // does not form between pH 1 and 10